Proceedings of the ASME 2023
50th Annual Review of Progress in
Quantitative Nondestructive Evaluation
QNDE2023
July 24-27, 2023, Austin, Texas

QNDE2023-118540

BATTERY HEALTH MONITORING USING GUIDED WAVE SIGNAL FEATURES

Dongjing Lao
University of Michigan-Shanghai Jiao Tong University Joint Institute, Shanghai Jiao Tong University, Shanghai, China

Yanfeng Shen
University of Michigan-Shanghai Jiao Tong University Joint Institute, Shanghai Jiao Tong University, Shanghai, China

Shaoteng Ren
Contemporary Amperex Technology Co., Limited, Fujian, China

Si Lin
Contemporary Amperex Technology Co., Limited, Fujian, China

Fenglin Zhang
Contemporary Amperex Technology Co., Limited, Fujian, China

ABSTRACT

The high-speed development of the new energy industry and the renewable energy facilities have made battery energy storage critical for Electric Vehicles (EVs) and large-scale Energy Storage Systems (ESSs). However, the complexity of the internal chemical reactions and the uncertainty of the external service environment seriously affect the reliability of batteries. Therefore, Battery Management Systems (BMS) have become essential to monitor battery health and performance, detect potential issues at an early stage, improve safety, and reduce costs associated with battery maintenance and replacement. This paper proposes a Battery Health Monitoring (BHM) system based on guided wave signal features to monitor and predict State of Charge (SOC), State of Health (SOH), and Remaining Useful Life (RUL) of batteries. A data collection system is developed to realize the integration of wave generation and reception, with subsequent feature extraction of the recorded ultrasound signals and characterization in different forms, enabling the prediction of battery health status and early alert of rapid battery capacity deterioration. The proposed method is based on time-frequency analysis of ultrasonic responses and weighted averaging algorithms for signal feature extraction, which facilitates the acquisition of indicative trends corresponding to battery SOC, SOH, and RUL variations. Experimental results indicate that the system can achieve real-time monitoring of battery SOC cycles, obtain battery SOH trends and health warnings of severe battery aging, and accurately predict the decay rate of the standard battery capacity to achieve RUL estimation, thus demonstrating the excellent evaluating capability of the active sensing method in battery health monitoring.

Keywords: battery health monitoring; guided waves; active sensing; signal processing; monitoring system

1. INTRODUCTION

The rapid development of the new energy industry and the renewable energy facilities have highlighted the importance of battery energy storage systems. These systems find extensive application in Electric Vehicles (EVs) and large-scale Energy Storage Systems (ESSs) [1, 2]. However, the reliability and safety of batteries are critical to their proper functioning and effectiveness in these applications. The complexity of the internal chemical reactions and the uncertainty of the external service environment impose significant challenges to achieving a reliable and safe operation. Failure of batteries can lead to huge economic losses and even pose significant safety risks, such as unstable voltage statuses, sudden power losses, and violent combustions [3, 4]. To mitigate these risks, Battery Management Systems (BMSs) have become essential tools for ensuring the proper functioning of batteries, detecting potential issues, improving safety, and reducing costs associated with battery maintenance and replacement.

Battery Health Monitoring (BHM) is a critical aspect of ensuring the safe and reliable operation of batteries, which can be classified into two levels, namely, battery-level and system-level monitoring [5]. System-level monitoring can be further categorized into offline and online fashions. Offline monitoring involves the use of a simplified circuit model to simulate the transient response of the battery and evaluate battery performance through data post-processing. Online monitoring relies on various sensors placed in the battery pack to collect information during vehicle operation, such as gas, temperature, pressure, voltage, current, and impedance of the batteries to

perform prognostics and health management as well as failure mode judgment [6–12]. Nevertheless, more advanced BMS are currently used to evaluate and identify the State of Charge (SOC) by analyzing the inherent physical quantities of the battery, such as voltage and current. The State of Health (SOH) and Remaining Useful Life (RUL), the most important parameters to evaluate the health condition of batteries, are difficult to evaluate (diagnose) and predict (prognose) properly.

Ultrasound has become an increasingly promising technique for measuring the health and performance of batteries [13]. The material properties of a battery change over time due to cycling and aging, and ultrasound propagation is also affected by these changes. Active sensing methods are widely used in the field of Structural Health Monitoring (SHM), and the investigation of ultrasound for battery monitoring has recently gained growing attention. For example, Davies et al. have shown that changes in SOC can be detected by differences in ultrasonic Time of Flight (TOF) [14]. More recently, Copley et al. created a model to demonstrate how changes in material properties during cycling affect ultrasonic reflection and how TOF measurements can reflect the SOC [15]. Most studies in this field have concentrated on detecting variations in SOC and SOH. It is evident that ultrasound can be used to identify dormant defects that worsen over the course of battery usage before leading to failures. In comparison to detecting changes in SOC and SOH, ultrasound is a practical approach to identify the accumulation of defects at an earlier stage than existing detection methods.

This paper presents a BHM system based on an active sensing method utilizing guided wave signals. In this study, the superb sensitivity and strong penetration capability of the ultrasonic wave method are fully employed to enable the monitoring and prediction of SOC, SOH, and RUL. This is achieved by the preferable features of ultrasonic guided waves, which embrace rich information of the internal structural changes of the batteries. This research initially develops a data collection system that realizes the integration of guided wave generation and reception, with subsequent feature extraction of the collected ultrasonic signals and characterization in different forms, thus enabling the predictive diagnostic information and early alarm of rapid battery capacity deterioration. The acquired ultrasonic signals are subjected to Short Time Fourier Transforms (STFT) to obtain the time-frequency spectra and extract the corresponding signal features. Finally, the characteristic trend profiles are plotted and evaluated in different forms, and the feature curves are fitted to the capacity variation readings to showcase the accurate prediction of abnormal batteries and warning of battery capacity deterioration.

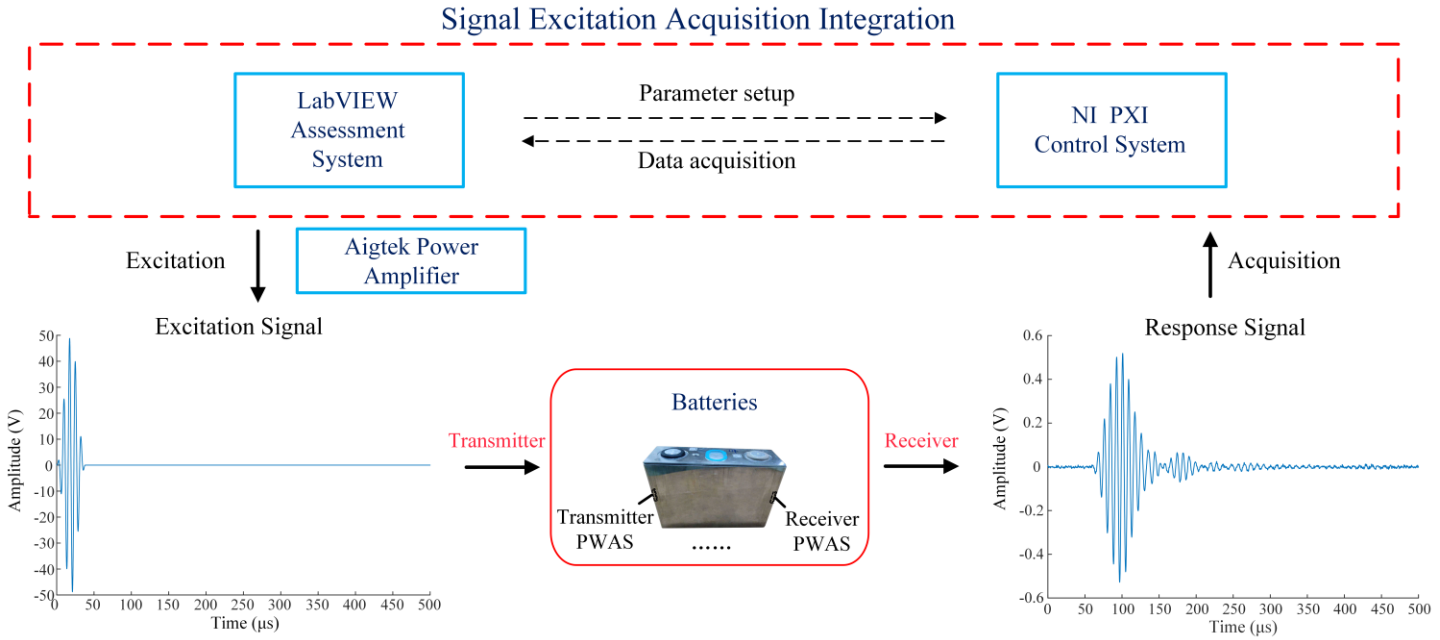

FIGURE 1: FRAMEWORK OF A GUIDED WAVE ACTIVE SENSING SYSTEM FOR BATTERY HEALTH MONITORING

2. ACTIVE SENSING BATTERY HEALTH MONITORING USING GUIDED WAVES

The charging and discharging of batteries involve a highly complex chemical reaction process that induces micro-level material changes, while causing only minimal changes in macroscopic physical quantities. As a result, passive monitoring methods have limited sensitivity in detecting changes in the internal structure of the battery. To overcome this limitation, an active monitoring approach is proposed for BHM, which employs guided waves for probing the internal structural evolution of the batteries. Via such an approach, a high level of sensitivity in detecting incipient changes can be achieved, enabling the accurate and reliable battery performance monitoring.

2.1 Construction of the active sensing system

FIGURE 1 depicts the framework of the proposed active sensing battery monitoring system, comprised of four parts: the control system for exciting and recording ultrasonic signals, Piezoelectric Wafer Active Sensors (PWASs) for wave field generation and reception, the target battery samples for testing, and the assessment system with implemented algorithm for processing and extracting quantitative signal features. The control system, based on the National Instruments (NI) PXI platform, contains a PXI chassis (PXIe-1071), a PXI controller (PXIe-8861), a PXI waveform generator (PXIe-5413), and a PXI oscilloscope (PXIe-5105). The assessment system is integrated into the PXI controller through the LabVIEW platform to allow real-time control of the PXI waveform generator and the PXI oscilloscope, resulting in an integrated data acquisition system for signal generation, reception, and post-processing.

The BHM system operates in the following manner: first, the ultrasonic excitation signal is parameterized and excited by the PXI waveform generator based on the application environment and the size of the battery; second, the energy of the excitation signal is amplified by an Aigtek power amplifier (ATA-4014) and applied to the electrode of the transmitter; thereafter, the transmitter PWAS generates ultrasonic guided wave field propagating through shell and interacting with the battery core at the same time; subsequently, the ultrasonic response signal, which contains rich internal information about the battery, is captured by the receiver PWAS and recorded by the PXI oscilloscope; finally, the data is processed at the assessment system implemented in the LabVIEW Graphical User Interface (GUI), enabling the diagnosis and prognosis of the SOC, SOH, and RUL of the monitored batteries.

In this way, the active sensing BHM system allows the integrated excitation and acquisition of ultrasonic guided wave signals, enabling simultaneous health monitoring of multiple battery samples in an efficient and reliable manner at a considerably low cost.

2.2 BHM experimental setup

In this research, a full-cycle battery health monitoring experiment was conducted over a period of more than two months. Two batteries with identical initial conditions as comparative samples were subjected to continuous charging and discharging to induce capacity decay from 100% to 80%. The test was conducted at Contemporary Amperex Technology Co., Limited (CATL), and the target battery samples were selected from CATL's power battery cells. To accelerate battery degradation, continuous charge/discharge tests were performed on the batteries with aluminum shells (shell dimensions: 221 mm *102 mm *33 mm) in a constant temperature test chamber (1200L) at 60°C. Due to confidentiality requirements, the details of the field test setup cannot be disclosed in the current paper. FIGURE 2 presents the experimental setup model built in the laboratory.

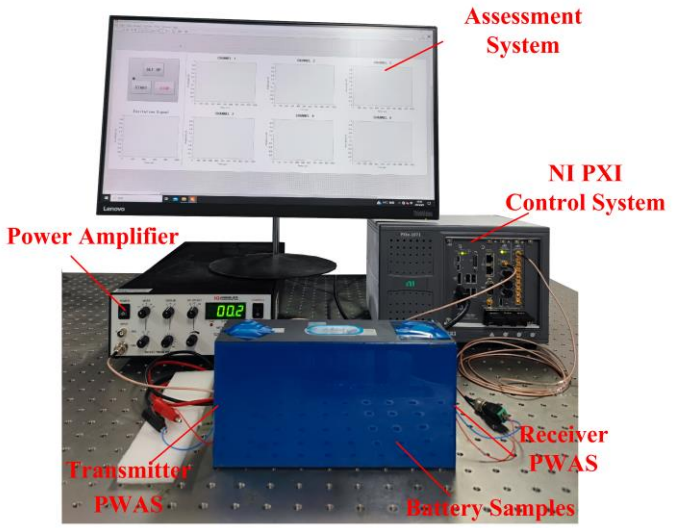

FIGURE 2: EXPERIMENTAL SETUP

FIGURE 3 illustrates the LabVIEW assessment system GUI used for parameter setting in the experiment, and the parameters of the experiment were displayed. To reduce dispersion effects and simplify analysis, a 100 Vpp five-count Hanning window modulated sine tone burst signal centered at 130 kHz (as shown in FIGURE 1) was applied. The excitation signal was amplified using the Aigtek power amplifier to obtain a 100 Vpp signal, since only 2 Vpp of excitation signal could be excited by the PXI waveform generator. The NI PXI control system was configured to transmit the excitation signal with a duration of 1000 μs to the actuator using the PXI waveform generator, with a sampling frequency of 20 MHz. The response signal with a duration of 1000 μs was captured from the receiver PWAS using the PXI oscilloscope with a sampling frequency of 10 MHz. To eliminate the noise generated by the complex power environment, the ultrasonic response data were obtained by averaging 20 sets of acquisitions at 500 ms intervals. The ultrasonic response data were recorded every 60,000 ms, i.e., one set of data per minute.

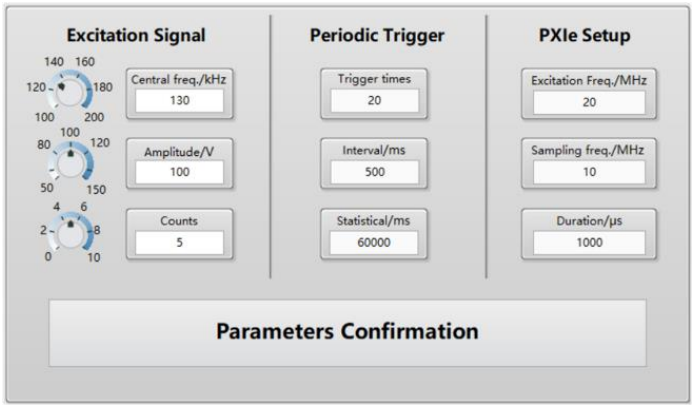

FIGURE 3: PARAMETER SETTING GUI

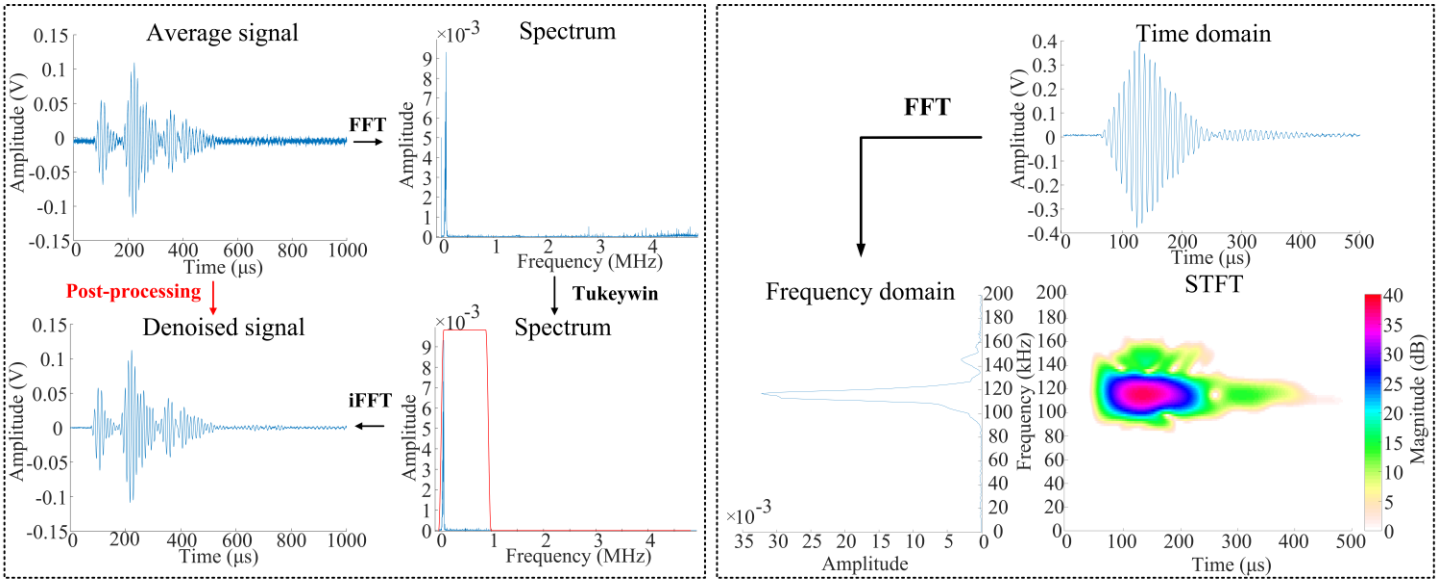

FIGURE 4: SIGNAL PROCESSING METHOD: (A) SIGNAL CONDITIONING AND RECONSTRUCTION; (B) TIME-FREQUENCY SPECTRUM AFTER STFT OPERATION FOR SIGNAL FEATURE EXTRACTION

3. ULTRASONIC SIGNAL FEATURE EXTRACTION

While the previous section explained the experimental setup and data acquisition process, this section focuses on the post-processing and feature extraction of the ultrasonic response signal data. The ultrasonic features extracted from the data are analyzed using various forms of characteristics to establish a correlation between them and the physical status of the battery. This correlation helps in achieving monitoring, diagnosis, and prognosis of the battery health condition.

3.1 Signal conditioning and reconstruction

In complex power equipment environments, ultrasonic signals were subject to electromagnetic interference (EMI) and mutual inductive coupling effects, while the low signal amplitude received by the receiver can be impacted by noisy interference, ultimately compromising the accuracy of signal feature extraction. Therefore, further signal conditioning is required to improve the quality of the ultrasonic response signals, as shown in FIGURE 4(a). In this signal conditioning step, the initial average signal was subjected to Fast Fourier Transform (FFT) analysis to derive a spectrum, which revealed the presence of distinct DC components, a 50Hz commercial electricity operating frequency, and high-frequency components. A Tukey window was then applied to the spectrum for bandpass filtering to retain frequency components between 50Hz and 1MHz, and the denoised signal was obtained by Inverse Fast Fourier Transform (IFFT) of the filtered spectrum back to the time domain. This process eliminated zero drifts and high-frequency noises, thus improving the quality of the ultrasonic sensing signal.

The ultrasonic signal is sensitive to the structural components' variations of the battery. Such sensitivity is brought about by the distinctive phenomenon like mode conversion, contact acoustic nonlinearity (CAN), and fluid-structure interaction. In the time domain, multiple wave packets or mode superposition may be present. However, conventional FFT data contain only the spectral information, disregarding the temporal dimension. In contrast, the time-frequency analysis shown in FIGURE 4(b) was employed STFT, embracing the features in both time and frequency domains to reconstruct the ultrasonic response signal and prepare for feature extraction. It is worth noting that the high-frequency components were absorbed by the liquid and plastic materials inside the battery, resulting in a decrease in the center frequency of the response signal.

3.2 Signal feature extraction algorithm

In this study, a weighted averaging algorithm was developed to extract signal key features from the time-frequency spectrum. These features were obtained from difference perspectives, including nominal TOF, center frequency, and total energy. The corresponding formulas are presented below:

1. Weighted average TOF (T_w)

$$T_w = \iint tM(f,t)dfdt \,/\, \iint M(f,t)dfdt \tag{1}$$

2. Weighted average central frequency (F_w)

$$F_w = \iint fM(f,t)dfdt \,/\, \iint M(f,t)dfdt \tag{2}$$

3. Weighted energy (E_w)

$$E_w = \iint M^2(f,t)dfdt \tag{3}$$

where $M(f,t)$ represents the pixel magnitude of each coordinate point in the time-frequency spectrum; f denotes the value on the frequency axis corresponding to each pixel; t stands for the value along the temporal axis.

4. RESULTS AND DISCUSSION

FIGURE 5 shows the experimental results of two comparative battery samples. The cycle life of a battery is defined as the number of cycles it can undergo from continuous charging and discharging until its capacity fades to 80%. The figure clearly indicates a significant difference in the service life of the two batteries despite being under the same initial condition. There is a discrepancy of about 70 charge/discharge cycles in between.

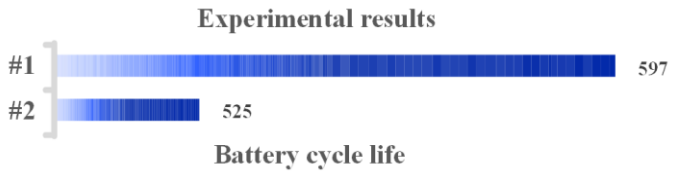

FIGURE 5: CYCLE LIFE OF THE MONITORED BATTERIES

4.1 Feature trend analysis

The ultrasonic signal features were calculated with a time interval of one minute, using the weighted averaging algorithm. FIGURE 6 presents the trend of these features for both batteries over their cycle life, with the number of charge cycles as the horizontal axis. Both batteries exhibited similar feature trends. The weighted average TOF increased gradually over time. In contrast, the weighted average central frequency and the weighted energy decreased gradually, with instability occurring at high degradation.

The gradual increase in TOF can be attributed to the fluid-structure interaction caused by the presence of electrolyte inside the battery, as well as by the pressure variation from the battery core. As the battery undergoes long-term chemical reactions, the increase in electrolyte concentration and squeezing pressure from the battery core lead to a decrease in the propagation speed of ultrasonic guided waves in the battery shell, resulting in the observed rise in TOF.

Due to the same battery status evolution, the weighted average central frequency of the ultrasonic response signal gradually decreases over the battery's cycle life, with instability occurring at high charge cycles. Additionally, when the battery reaches a highly debilitated capacity, unstable by-products from the chemical reactions would affect its stability, causing the F_w features of the ultrasonic response signal to jitter violently.

Regarding the weighted energy, the feature tends to rise in the early charge cycle and then gradually decrease. The optimal stable internal reaction of the battery occurs at approximately 50 cycles, after which incomplete reactions and by-products form gradually and incrementally. During this period, the battery core boundary regions come in contact with the shell and squeeze each other due to expansion, leading to a change in the physical properties of the waveguide. Ultrasonic guided waves are partially transmitted into the electrolyte and the core, resulting in a gradual decrease in the weighted energy. Once the weighted energy drops below $0.2*10^6$, the battery enters a highly degraded condition, and a battery safety warning is triggered.

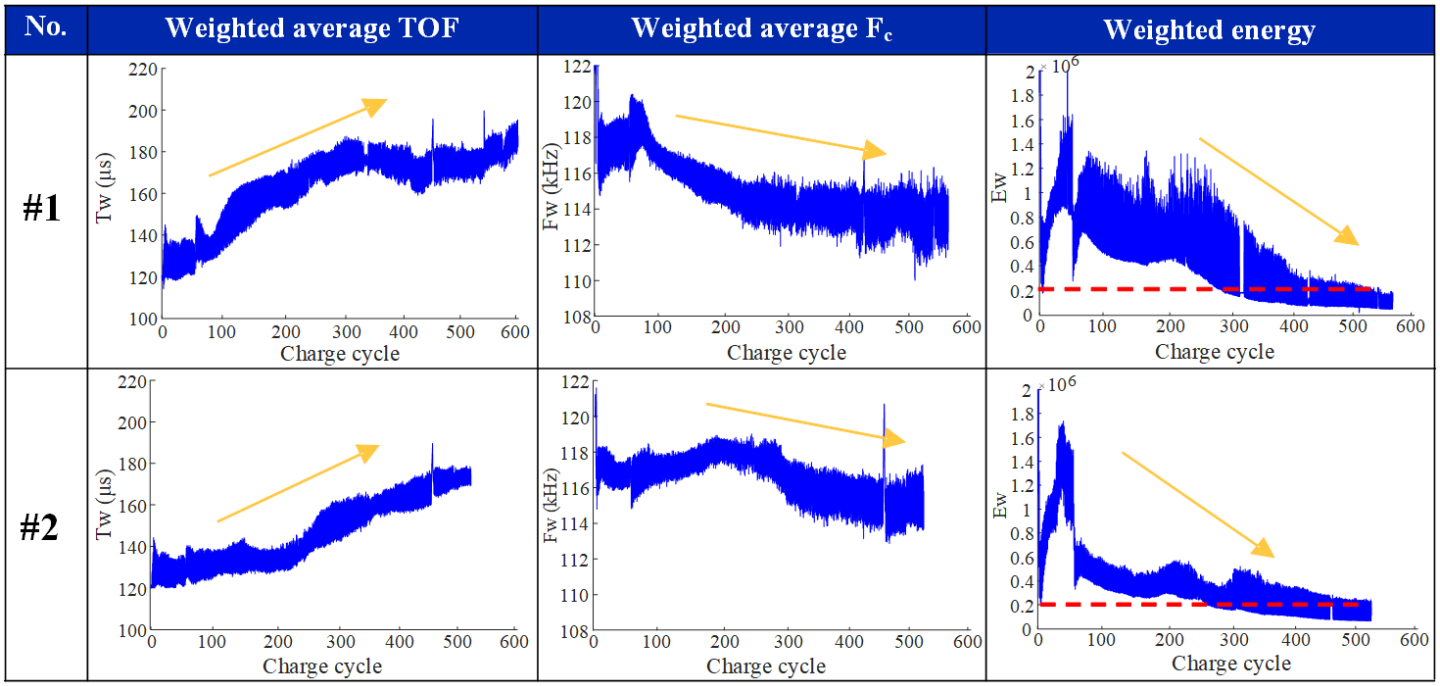

FIGURE 6: THE TENDENCY OF ULTRASONIC RESPONSE SIGNAL FEATURES OF BATTERIES #1 and #2

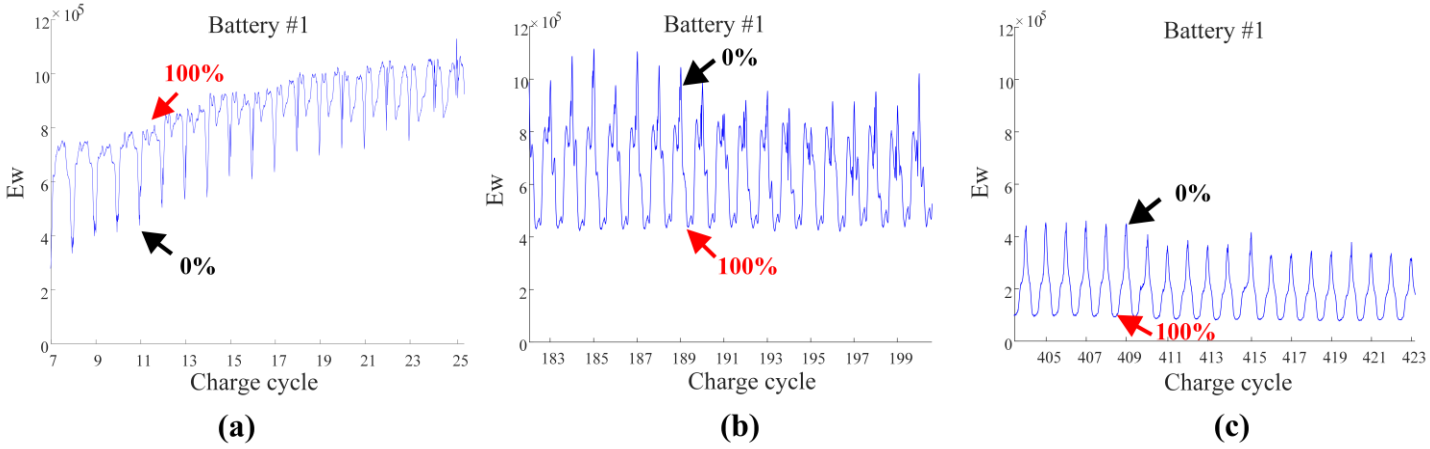

FIGURE 7: TREND OF WEIGHTED ENERGY OF THE BATTERY #1 AT EACH NUMBER OF CHARGE CYCLES

All three features, namely the weighted average TOF, weighted average central frequency, and weighted energy, exhibit a clear correlation with the battery SOH. By combining these features, a more accurate determination of when the battery enters a high level of degradation can be made, enabling advance prediction of battery failure. It is noteworthy that the weighted energy contains more critical information about battery degradation compared to the other two features

4.2 Correlation between weighted energy and capacity

Ultrasonic signals, containing battery variation information, were represented by the weighted energy. FIGURE 7 presents the trend of the weighted energy for battery #1 at each charge cycle obtained by Eq. (1). The E_w variations were clearly observable during the charging and discharging cycles, exhibiting a cyclic pattern behaving like a “battery breathing” procedure. The figure marks the E_w of 100% and 0% SOC corresponding to a single cycle. In FIGURE 7(a), representing the early stage of the battery charge cycle, the single cycle SOC displayed an "M" shape, with the lowest value associated with the fully discharged state of the battery. The E_w of the battery increased during the charging process, attained a maximum value, subsequently decreased, and ultimately reached an intermediate depressed position that indicates the battery has been fully charged. FIGURE 7(b) shows that as the battery undergoes repeated charge-discharge cycles, the E_w corresponding to 0% SOC gradually increases relative to that of 100% SOC, while the depressions that form the "M" shape become more prominent. Finally, the E_w of the single cycle SOC after the high charge cycle formed a "U" shape as shown in FIGURE 7(c). The higher the battery power content, the lower the E_w of the ultrasonic response signal. From the above, it can be concluded that the E_w change of ultrasonic response signals and the change of battery SOC are in agreement, enabling clear SOC identification.

The E_w change characteristics at 100% and 0% SOC were found for correlating to battery degradation. To demonstrate this relationship, FIGURE 8 displays the capacity degradation curves of the battery and the 100% - 0% SOC curves extracted from the E_w. Additionally, the average SOC characteristics were obtained from the energy SOC using Eq. (4).

$$E_{w-AveSOC} = \frac{E_{w-100\%SOC} + E_{w-0\%SOC}}{2} \tag{4}$$

where $E_{w-100\%SOC}$ and $E_{w-0\%SOC}$ are the E_w at the same charge cycle corresponding to the 100% and 0% SOC, $E_{w-AveSOC}$ is the average SOC characteristic, shown as the red line, representing average SOC in the weighted energy SOC curves.

The E_w change characteristics at 100% and 0% SOC were found to be linked to battery degradation. Hence, to illustrate this relationship, FIGURE 8 shows the capacity degradation curves of the battery measured by standard electronic equipment and the 100% - 0% SOC curves extracted from the E_w. The trend of the capacity and average SOC curves is quite similar, with an initial increase, followed by a gradual decrease until battery failure. The 100% capacity in the capacity curves is based on the initial condition of the battery, where the capacity may appear to be greater than 100% due to the battery reaching its optimal state in the early charge cycles. Therefore, to accurately analyze capacity decline, it is better to consider the decline from 100% to 80% after the battery reaches its optimal state, as shown in FIGURE 8 for the E_w capacity normalization curve.

The truncated average SOC curves were first subjected to a max-min normalization operation using Eq. (5). Next, the obtained normalized average SOC curves were aligned with the capacity curves, and the vertical coordinate was normalized to the capacity. Finally, the Edit Distance on Real Sequences(EDR) of the two curves was calculated using the Euclidean distance, as in Eq. (6). The study found a high EDR of more than 98% for both battery samples. The trend of the E_w average SOC curves of the ultrasonic signal can be used to predict and prognose the degradation rate of battery capacity for batteries with large differences in battery cycle life, eventually enabling battery failure alarms.

$$E_{w-norm} = \frac{E_{w-AveSOC} - \min(E_{w-AveSOC})}{\max(E_{w-AveSOC}) - \min(E_{w-AveSOC})} \quad (5)$$

$$EDR_{C-E_w} = 1 - D_E(C, E_w) = 1 - \frac{1}{n}\sum_{k=1}^{n} |C_k - E_{wk}| \quad (6)$$

where EDR_{C-E_w} is the EDR between the capacity and E_w average SOC. $D_E(C, E_w)$ represents the Euclidean distance between two one-dimensional curves.

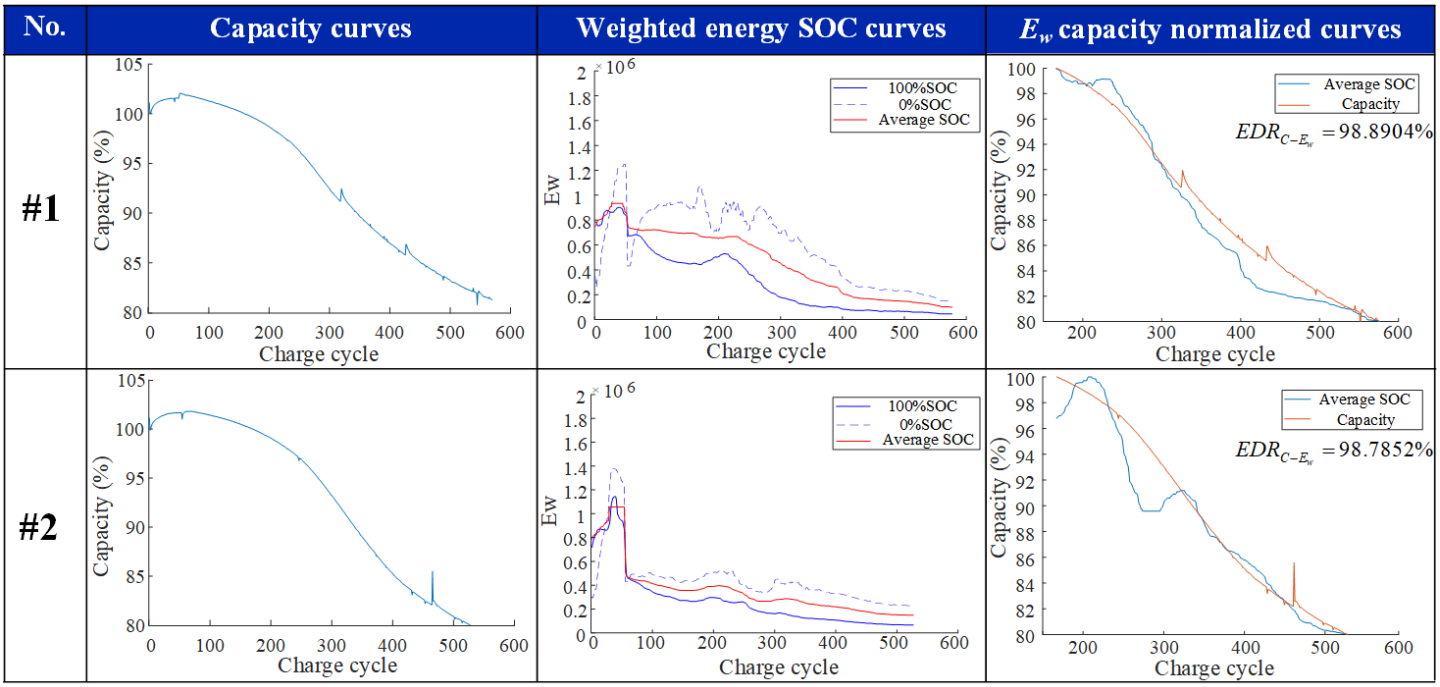

FIGURE 8: CORRESPONDENCE BETWEEN WEIGHT ENERGY SOC CURVE AND CAPACITY CURVE

5. CONCLUSION

In this study, an active ultrasonic guided wave sensing approach for battery health monitoring is proposed, suitable for giving early alarms of battery failures in EVs and large-scale ESSs. The system integrates interrogative signal generation and acquisition, as well as quantitative battery health evaluation, including SOC, SOH, capacity decay, and failure alarm. The proposed method employs STFT and weighted average algorithms for ultrasonic signal reconstruction and feature extraction, enabling the tracing of charging cycle feature trends corresponding to battery SOC, SOH, and RUL. The system is capable of real-time monitoring of multiple batteries of different sizes. Experimental results demonstrate the system's ability to provide real-time demonstration of battery SOC cycle changes, obtain battery SOH trends and health warnings of severe battery aging, and accurately predict the decay rate of the standard battery capacity to achieve RUL estimation. The results highlighted the active ultrasonic sensing method's excellent monitoring capability in battery health management.

ACKNOWLEDGEMENTS

This study is supported by the Contemporary Amperex Technology Co., Limited. It should be emphasized that the technology described in this paper is the subject of a patent owned by the support company. As such, it cannot be used or replicated without the express permission of the company. Any unauthorized use or replication of this technology may result in legal action.

REFERENCES

[1] E. Karden, S. Ploumen, B. Fricke, T. Miller, and K. Snyder, “Energy storage devices for future hybrid electric vehicles,” *Journal of Power Sources*, vol. 168, no. 1, pp. 2–11, May 2007, doi: 10.1016/j.jpowsour.2006.10.090.

[2] Q. Zhang, X. Li, C. Zhou, Y. Zou, Z. Du, M. Sun, Y. Ouyang, D. Yang and Q. Liao, , “State-of-health estimation of batteries in an energy storage system based on the actual operating parameters,” *Journal of Power Sources*, vol. 506, p. 230162, Sep. 2021, doi: 10.1016/j.jpowsour.2021.230162.

[3] M. Armand and J.-M. Tarascon, “Building better batteries,” *Nature*, vol. 451, no. 7179, pp. 652–657, Feb. 2008, doi: 10.1038/451652a.

[4] S. C. Levy, “Safety and reliability considerations for lithium batteries,” *Journal of Power Sources*, vol. 68, no. 1, pp. 75–77, Sep. 1997, doi: 10.1016/S0378-7753(96)02622-5.

[5] S. M. Rezvanizaniani, Z. Liu, Y. Chen, and J. Lee, “Review and recent advances in battery health monitoring and prognostics technologies for electric vehicle (EV) safety and

mobility," *Journal of Power Sources*, vol. 256, pp. 110–124, Jun. 2014, doi: 10.1016/j.jpowsour.2014.01.085.

[6] Y. Fernandes, A. Bry, and S. de Persis, "Identification and quantification of gases emitted during abuse tests by overcharge of a commercial Li-ion battery," *Journal of Power Sources*, vol. 389, pp. 106–119, Jun. 2018, doi: 10.1016/j.jpowsour.2018.03.034.

[7] F. Tao, W. Zhang, D. Guo, W. Cao, L. Sun, and F. Jiang, "Thermofluidic modeling and temperature monitoring of Li-ion battery energy storage system," *Applied Thermal Engineering*, vol. 181, p. 116026, Nov. 2020, doi: 10.1016/j.applthermaleng.2020.116026.

[8] J. Peng, S. Jia, S. Yang, X. Kang, H. Yu, and Y. Yang, "State estimation of lithium-ion batteries based on strain parameter monitored by fiber Bragg grating sensors," *Journal of Energy Storage*, vol. 52, p. 104950, Aug. 2022, doi: 10.1016/j.est.2022.104950.

[9] J. Xi, J. Li, H. Sun, T. Ma, L. Deng, N. Liu, X. Huang and J. Zhang, "In-situ monitoring of internal temperature and strain of solid-state battery based on optical fiber sensors," *Sensors and Actuators A: Physical*, vol. 347, p. 113888, Nov. 2022, doi: 10.1016/j.sna.2022.113888.

[10] K.-H. Shin, C.-S. Jin, J.-Y. So, S.-K. Park, D.-H. Kim, and S.-H. Yeon, "Real-time monitoring of the state of charge (SOC) in vanadium redox-flow batteries using UV–Vis spectroscopy in operando mode," *Journal of Energy Storage*, vol. 27, p. 101066, Feb. 2020, doi: 10.1016/j.est.2019.101066.

[11] M. A. Roscher, R. M. Kuhn, and H. Döring, "Error detection for PHEV, BEV and stationary battery systems," *Control Engineering Practice*, vol. 21, no. 11, pp. 1481–1487, Nov. 2013, doi: 10.1016/j.conengprac.2013.07.003.

[12] A. Szumanowski and Y. Chang, "Battery Management System Based on Battery Nonlinear Dynamics Modeling," *IEEE Transactions on Vehicular Technology*, vol. 57, no. 3, pp. 1425–1432, 2008, doi: 10.1109/TVT.2007.912176.

[13] P. Ladpli, F. Kopsaftopoulos, and F.-K. Chang, "Estimating state of charge and health of lithium-ion batteries with guided waves using built-in piezoelectric sensors/actuators," *Journal of Power Sources*, vol. 384, pp. 342–354, Apr. 2018, doi: 10.1016/j.jpowsour.2018.02.056.

[14] G. Davies, K. W. Knehr, B. Van Tassell, T. Hodson, S. Biswas, A. G. Hsieh and D. A. Steingart, "State of Charge and State of Health Estimation Using Electrochemical Acoustic Time of Flight Analysis," *J. Electrochem. Soc.*, vol. 164, no. 12, pp. A2746–A2755, 2017, doi: 10.1149/2.1411712jes.

[15] R. J. Copley, D. Cumming, Y. Wu, and R. S. Dwyer-Joyce, "Measurements and modelling of the response of an ultrasonic pulse to a lithium-ion battery as a precursor for state of charge estimation," *Journal of Energy Storage*, vol. 36, p. 102406, Apr. 2021, doi: 10.1016/j.est.2021.102406.

[16] M. Jacoby, "Burning batteries," *Chemical & engineering news*, vol. 85, no. 51, pp. 26–28, 2007.